Available online at www.sciencedirect.com
SCIENCE DIRECT®
PERGAMON
International Journal of Heat and Mass Transfer 46 (2003) 3841–3851
International Journal of HEAT and MASS TRANSFER
www.elsevier.com/locate/ijhmt

Structures of scalar transport in 2D transitional jet diffusion flames by LES

Y. Liu [a], K.S. Lau [b], C.K. Chan [c,*], Y.C. Guo [a], W.Y. Lin [a]

[a] Department of Engineering Mechanics, Tsinghua University, Beijing 100084, China
[b] Department of Applied Physics, The Hong Kong Polytechnic University, Hung Hom, Kowloon, Hong Kong
[c] Department of Applied Mathematics, The Hong Kong Polytechnic University, Hung Hom, Kowloon, Hong Kong

Received 30 August 2002; received in revised form 28 March 2003

Abstract

In this paper, large eddy simulation of a two-dimensional spatially developing transitional free methane diffusion jet at moderate Reynolds number is performed. The solver of the governing equations is built based on a projection method and time integration is carried out using a second-order Adams–Bashforth scheme. A dynamic eddy viscosity model is utilized for the turbulent subgrid scale terms and a similar dynamic method is applied for modeling the filtered reaction rate. The direct solver for pressure correction Poisson equation is based on the Buneman variant of cyclic odd–even reduction algorithm. A reduced four-step chemical kinetic mechanism is applied for the simulation of methane combustion. Ignition process is well described by the simulation. Detailed description of transient vortical structures in the entire flow field is given along with transient vortex–flame interactions. The development of a diffusion jet flame is found to involve two distinct phases of ''turbulence dominated'' and ''reaction dominated'' respectively. The ''turbulence dominated'' phase exists only for a very short time at the initial stage of the flame.

Keywords: Large eddy simulation; Planar jet; Turbulent combustion; Diffusion flame

1. Introduction

Turbulent combustion is a common phenomenon that has been the focus of many investigations [1–4]. Among numerous types of turbulent flames, diffusion jet flame is of particular interest for its wide application in engineering. Planar jet is a typical shear flow involving intensive interaction between neighboring streams and having typical vortical characteristics of turbulent flows [5,6]. The complex vortex–flame interaction in a reactive jet flow is a major factor that influences the development of a turbulent flame. Experimental study is an intuitive and direct method to clarify structures of turbulent flames and numerous researches have been performed [7,8]. Although numerical simulation provides a useful tool for the understanding of the detailed structures especially for the transient evolution, the chemical kinetic mechanism of combustion process remains the main challenge for numerical simulations. For the lowest hydrocarbon, methane, the full mechanism of combustion has been identified as having more than 300 elementary reactions and over 30 species [9]. However, such a complex mechanism is extremely difficult to numerically simulate due to the large number of species and the wide range of length and time scales. In recent years, models of reduced kinetics have been developed and successfully applied to both premixed and non-premixed methane flames.

For numerical simulation of turbulent combustion, direct numerical simulations (DNS) have been applied to simple flow configurations. However, DNS is quite difficult to be extended to complex turbulent flames due to the large computational scale. While numerical simulations based on the Reynolds averaged Navier–Stokes (RANS) technique have also been adopted by many

* Corresponding author. Tel.: +852-2766-6919; fax: +852-2362-9045.
E-mail address: ck.chan@polyu.edu.hk (C.K. Chan).

0017-9310/03/$ - see front matter © 2003 Elsevier Ltd. All rights reserved.
doi:10.1016/S0017-9310(03)00193-5

Nomenclature

b_0	half jet width
C	turbulence SGS model coefficient
C_M	concentration of the third body
C_r	combustion SGS model coefficient
d	width of the jet exit
G	filtering function
k	reaction rate constants
K	equilibrium constants of reaction rate
p	pressure
P_0	atmospheric pressure
Pr	Prandtl numbers
Q	reaction heat
R	universal gas constant
Re	Reynolds number
Sc	Schmidt numbers
t	time
T	temperature
u, v	velocity components
u', v'	fluctuating velocity components
U_{con}	area weighted mean stream-wise velocity
W	molecular weight
$\overline{W}$	mean molecular weight
x	stream-wise spatial coordinates
y	transverse spatial coordinates
Y_i	mass fraction of species i

Greek symbols

ω	reaction rate
ρ	density
μ_T	subgrid turbulent viscosity
η_i	catalytic efficiency of species i
μ	molecular viscosity

researchers, they fail to capture directly the dynamics of the coherent eddies, due to the non-linear, non-local and intensively anisotropic properties of fully developed turbulent combustion. Furthermore, RANS methods are time-averaged and are generally not capable of capturing transient behaviors of flow patterns. In the past few years, large eddy simulation (LES) was used widely [10,11] for the simulation of turbulent combustions. In LES, each flow field variable is "filtered" into a large-scale and a small-scale component. As large-scale structures carry most of the kinetic energy and are responsible for most of the turbulent flux, they are dependent on the geometry of the flow field and are computed explicitly.

Although turbulence is by the nature three-dimensional, 2D structures are still the object of many research works. In particular, the well-documented quasi-two-dimensional large-scale structures in the planar jet contribute to the understanding of vortex–flame interactions in the diffusion flame. The assumption of two-dimensional flow precludes the vortex stretching mechanism, but does allow for enhanced mixing and unpredictability, which are the two important features of turbulent flow. In addition, the near-field transitional mixing in turbulent jets seems to be dominated by two-dimensional large-scale structures, which can be captured in 2D simulations. A 2D simulation also makes calculations more affordable and is reasonable to be a logical first step in the simulation of turbulent flame. In this paper, simulation of a two-dimensional spatially developing transitional free methane diffusion jet at moderate Reynolds number is performed by means of LES using a dynamic subgrid scale eddy viscosity model. Transient structures of the turbulent flame in the entire flow field as well as transient vortex–flame interactions are presented.

2. Formulation and numerical procedure

2.1. Reaction mechanics

The reduced chemical kinetic mechanism of methane considered in this paper is the reduced four-step mechanism of Seshadri and Peters [12]. Such a mechanism is reduced from a set of 22 elementary reactions with steady-state assumption for O, OH, HO_2, CH_3, CH_2O and are shown as follows:

(I) $CH_4 + 2H + H_2O \rightarrow CO + 4H_2$
(II) $CO + H_2O \leftrightharpoons CO_2 + H_2$
(III) $H + H + M \rightarrow H_2 + M$
(IV) $O_2 + 3H_2 \leftrightharpoons 2H + 2H_2O$

The reaction rates are expressed in terms of the rates of the flowing elementary reactions, where

$$\omega_I = k_{11} C_{CH_4} C_H, \tag{1}$$

$$\omega_{II} = (k_{10}/K_3)(C_H C_{H_2})(C_{CO} C_{H_2O} - C_{CO_2} C_{H_2}/K_{II}), \tag{2}$$

$$\omega_{III} = k_5 C_{O_2} C_H C_M, \tag{3}$$

$$\omega_{IV} = k_1 C_H (C_{O_2} - C_H^2 C_{H_2O}^2/(C_{H_2}^3 K_{IV})). \tag{4}$$

Based on Seshadri and Peters [12], the reaction rate constants are expressed in the Arrhenius form $k_j = A_j T^{n_j} \exp(-E_j/RT)$ and the equilibrium constants are given by

Table 1
Catalytic efficiencies of different species

Species	CH_4	H_2O	CO_2	H_2	CO	O_2	N_2	Others
Catalytic efficiency	6.5	6.5	1.5	1.0	0.75	0.4	0.4	1.0

$$K_3 = 0.2675T^{-0.0247}\exp(15083/RT), \tag{5}$$

$$K_{II} = 3.828\times10^{-5}T^{0.8139}\exp(9839/RT), \tag{6}$$

$$K_{IV} = 11.283T^{-0.2484}\exp(11400/RT). \tag{7}$$

The concentration of the third body C_M can be written in terms of the catalytic efficiency η_i of species i and its molecular weight W_i as

$$C_M = (p\overline{W}/RT)\sum_{i=1}^{N_s}\eta_i Y_i/W_i, \tag{8}$$

where R is the universal gas constant, p is pressure, T is temperature and $\overline{W}$ is the mean molecular weight. The catalytic efficiencies for the different species are given in Table 1 [9].

2.2. Configuration of the simulation

In this paper, a planar jet is formed by admitting a pure methane stream into a quiescent air environment with a uniform velocity through a gap between two infinitely large plates as shown schematically in Fig. 1. The width of the gap, $d = 2b_0$, is 0.02 m. The stream-wise and transverse spatial coordinates are denoted by x and y respectively. The computational domain is rectangular of size 0.4 m × 0.34 m. Two staggered grids of 131×121 and 259×249 nodes were tested. The latter grid configuration provided grid independent results and was therefore adopted for the simulation in this paper. The time step was chosen to be 1.0×10^{-6} s.

2.3. Governing equations

Filtered non-dimensionalised governing equations, including continuity, momentum, energy, and species transport equations are solved in Cartesian coordinates. The half jet width, initial velocity of the jet, and the thermal dynamic parameters along the centerline at the inlet are used for non-dimensionalisation, as shown in Table 2. Reynolds number based on these parameters is 6.6×10^3.

In LES of turbulent combustion, Favre filtering is commonly used to separate variables into large-scale components and subgrid-scale components. Favre filter is spatially density weighted with the formulation given as

$$\overline{\rho f(x_i,t)} = \bar{\rho}\tilde{f}(x_i,t) = \int_D \rho f(x',t)G(x_i-x',\Delta)\,dx', \tag{9}$$

where f refers to any unresolved variable, ρ is density, G is the filtering function and the sign "$\sim$" denotes Favre filtering.

In Cartesian tensor notation, the Favre filtered non-dimensionalised governing equations are obtained as follows:

$$\frac{\partial\bar{\rho}}{\partial t}+\frac{\partial\bar{\rho}\tilde{u}_j}{\partial x_j}=0, \tag{10}$$

$$\frac{\partial\bar{\rho}\tilde{u}_i}{\partial t}+\frac{\partial\bar{\rho}\tilde{u}_i\tilde{u}_j}{\partial x_j}=-\frac{\partial\bar{p}}{\partial x_i}+\frac{\partial m_{ij}}{\partial x_j}, \tag{11}$$

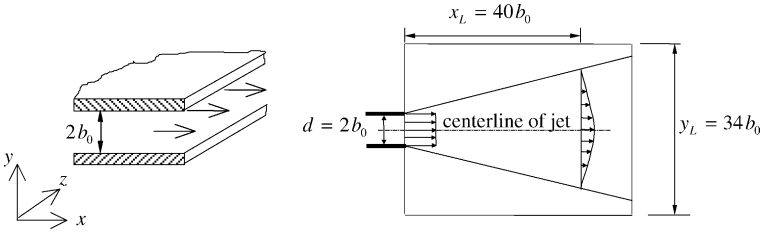

Fig. 1. Schematic diagram of the planar jet.

Table 2
Non-dimensionalisation of different quantities

Variables	x	y	u	v	u'	v'	t	ρ	c_p	p	μ	T	ω_α	Q_α
Scale	b_0	b_0	U_0	U_0	U_0	U_0	b_0/U_0	ρ_0	c_{p0}	$\rho_0U_0^2$	μ_0	T_0	ρ_0U_0/b_0	$c_{p0}T_0$

$$\frac{\partial \bar{\rho}\widetilde{Y}_s}{\partial t}+\frac{\partial \bar{\rho}\widetilde{Y}_s\tilde{u}_j}{\partial x_j}=\frac{\partial}{\partial x_j}\left(\frac{\mu^*}{Sc}\frac{\partial \widetilde{Y}_s}{\partial x_j}\right)+\bar{\omega}_s, \tag{12}$$

$$\frac{\partial \bar{\rho}\tilde{c}_p\widetilde{T}}{\partial t}+\frac{\partial \bar{\rho}\tilde{c}_p\widetilde{T}\tilde{u}_j}{\partial x_j}=\frac{\partial}{\partial x_j}\left(\frac{\mu^*\tilde{c}_p}{Pr}\frac{\partial \widetilde{T}}{\partial x_j}\right)+\bar{\omega}_\alpha Q_\alpha, \tag{13}$$

where

$$m_{ij}=\mu^*\left(\frac{\partial u_i}{\partial x_j}+\frac{\partial u_j}{\partial x_i}-\frac{2}{3}\delta_{ij}\frac{\partial u_k}{\partial x_k}\right) \tag{14}$$

and

$$\mu^*=\mu_{\mathrm{T}}+\bar{\mu}/Re. \tag{15}$$

The ideal gas state equation is satisfied as

$$\bar{\rho}=\frac{\bar{p}_0}{R\widetilde{T}\sum \widetilde{Y}_s/W_s}, \tag{16}$$

where u_i is the velocity component and $i=1$, 2 denote stream-wise and transverse directions respectively. μ is the molecular viscosity, μ_{T} is the subgrid turbulent viscosity, $Re=\rho_0U_0b_0/\mu_0$ is the Reynolds number and δ_{ij} is the Kronecher delta function. Y_s and W_s are the mass fraction and molecular weight of species s. Sc and Pr are Schmidt and Prandtl numbers, which are assumed to be equal to 0.72 in our calculations. $p_0=1.0135\times10^5$ Pa is the atmospheric pressure, R is the universal gas constant, $\bar{\omega}_s$ is the filtered chemical reaction rate of species s. The chemical reaction rate and the reaction heat of each reaction step are denoted by $\bar{\omega}_\alpha$ and Q_α respectively. As a reduced four-step reaction mechanism is adopted, α takes on values of I, II, III and IV as in Eqs. (1)–(4).

2.4. Turbulent SGS model

In this paper, a dynamic subgrid-scale eddy viscosity model [13] based on the standard Smagorinsky model [14] is adopted for the modeling of μ_{T}. The model coefficient, which is fixed in the Smagorinsky model, is treated dynamically. To perform this, a test-level filter is applied to the filtered N–S equations with generally twice the width of the grid-level filter.

After grid-level filtering of the governing equations, the subgrid scale stress term has the following form

$$\tau_{ij}=\bar{\rho}\widetilde{u_iu_j}-\bar{\rho}\tilde{u}_i\tilde{u}_j=\overline{\rho u_iu_j}-\overline{\rho u_i\rho u_j}/\bar{\rho}. \tag{17}$$

A standard Smagorinsky model [14] of τ_{ij} is to assume

$$\tau_{ij}-\tfrac{1}{3}\tau_{kk}\delta_{ij}=-2C\bar{\rho}\Delta^2|\widetilde{\mathbf{S}}|\left(\widetilde{S}_{ij}-\tfrac{1}{3}\widetilde{S}_{kk}\delta_{ij}\right), \tag{18}$$

where

$$\widetilde{S}_{ij}=\frac{1}{2}\left(\frac{\partial \tilde{u}_i}{\partial x_j}+\frac{\partial \tilde{u}_j}{\partial x_i}\right),\quad |\widetilde{\mathbf{S}}|=(2\widetilde{S}_{ij}\widetilde{S}_{ij})^{1/2}. \tag{19}$$

As suggested by Fureby [10], τ_{kk} may be modeled as

$$\tau_{kk}=2C_{\mathrm{I}}\bar{\rho}\Delta^2|\widetilde{\mathbf{S}}|^2, \tag{20}$$

where, Δ is the characteristic filter width and C is a fixed model constant. Erlebacher et al. [15] suggested that τ_{kk} may be ignored for $C_{\mathrm{I}}\ll C$.

Although widely adopted, the Smagorinsky model has some drawbacks such as incorrect prediction of the limiting behavior near a wall or in laminar flows and the inability to take into account of the transfer of energy from the small scales to the large scales with the fixed model constant. These drawbacks may be overcome by means of a dynamically determined model coefficient.

2.5. Combustion SGS model

Reaction rate is a complex function of the instantaneous (non-filtered) values of the reactive species and thermodynamic variables. Due to the intensive nonlinear interactions among reactive species, the closure of filtered reaction rate is more difficult than that of the turbulent SGS stress. Most of the developed SGS models for combustion require a large amount of computational effort. In this paper, a less computational intensive SGS combustion model, based on the dynamic similarity model of Jaberi and James [11], is adopted.

The dynamic similarity model is similar to the dynamic turbulent model, where the filtered reaction rate is decomposed as

$$\bar{\omega}=\overline{\omega(\phi)}=\omega(\bar{\boldsymbol{\phi}})+\lambda, \tag{21}$$

where $\bar{\boldsymbol{\phi}}$ represents the filtered values of the thermodynamic variables and species and $\lambda=\overline{\omega(\phi)}-\omega(\bar{\boldsymbol{\phi}})$ is the generalized SGS term. A similarity closure for this term is given by

$$\lambda=C_{\mathrm{r}}[\overline{\omega(\bar{\boldsymbol{\phi}})}-\omega(\bar{\bar{\boldsymbol{\phi}}})], \tag{22}$$

where the model coefficient, C_{r}, is evaluated by the dynamic method similar to the one used for the turbulent SGS stress. A test-level filter having filter width twice of that of the grid-level is applied, thus

$$\widehat{\bar{\omega}}=\omega(\hat{\bar{\boldsymbol{\phi}}})+\Lambda, \tag{23}$$

where Λ is the SGS term at the test level and can be obtained similar to Eq. (31) as

$$\Lambda=C_{\mathrm{r}}[\widehat{\overline{\omega(\bar{\boldsymbol{\phi}})}}-\omega(\bar{\bar{\boldsymbol{\phi}}})]. \tag{24}$$

The grid and test level SGS term are related by

$$\widehat{\omega(\bar{\boldsymbol{\phi}})}-\omega(\hat{\bar{\boldsymbol{\phi}}})=\Lambda-\hat{\lambda}, \tag{25}$$

and substituting Eqs. (22) and (24) into Eq. (25), an expression for C_{r} is obtained as

$$C_r = \frac{\widehat{\omega(\tilde{\phi})} - \omega(\hat{\tilde{\phi}})}{\widehat{\omega(\tilde{\phi})} - \omega(\hat{\tilde{\phi}})}. \quad (26)$$

2.6. Solution of the governing equations

A projection method, which treats pressure as an intermediate variable satisfying the continuity equation, is utilized in solving the governing equations. Equations for Y_s and T at the $(n+1)$th time step are initially solved explicitly from the values of the nth time step. The density at the $(n+1)$th time step is then calculated from the ideal gas equation. The momentum equations without the pressure term are solved to obtain the predicted velocity field $\vec{V}^*$. With this predicted velocity field, the Poisson equation for pressure is obtained and the term $\partial\rho/\partial t$ calculated with ρ^{n+1} and ρ^n. As solving the Poisson equation is very time consuming, an efficient solver is necessary. In this paper, a direct solver based on the Buneman variance of cyclic odd–even reduction algorithm [16] is used. With the pressure Poisson equation solved, the predicted velocity $\vec{V}^*$ is finally corrected to $\vec{V}^{n+1}$.

2.7. Initial and boundary conditions

The jet flow simulated in this study is a non-forced free jet. The initial condition of velocity is assumed to be isothermal and quiescent with both velocity components being zero,

$$\begin{cases} u = u_{\text{jet}} = 0.0 \text{ m/s}, \quad v = 0.0 \text{ m/s}, \\ Y_{CH_4} = 0.0, \quad Y_{\text{air}} = 1.0, \\ T = 298.15 \text{ K}, \\ \\ T = 1000 \text{ K}, \\ \quad b_0 \leqslant s \leqslant 2b_0, \quad y_{\text{center}} - 2b_0 \leqslant y \leqslant y_{\text{center}} + 2b_0. \end{cases} \quad (27)$$

For the inflow boundary, velocity is assumed to satisfy Dirichlet conditions with a top-hat profile.

$$\begin{cases} u = u_{\text{jet}} = 10.0 \text{ m/s}, \quad v = 0.0 \text{ m/s}, & \\ Y_{CH_4} = 1.0, \quad Y_{\text{air}} = 0.0, & y_{\text{center}} - b_0 \leqslant y \leqslant y_{\text{center}} + b_0, \\ T = 298.15 \text{ K}, & \\ u = u_{\text{co}} = 0.0 \text{ m/s}, \quad v = 0.0 \text{ m/s}, & \\ Y_{CH_4} = 0.0, \quad Y_{\text{air}} = 1.0, & \text{elsewhere.} \\ T = 298.15 \text{ K}, & \end{cases} \quad (28)$$

At lateral boundaries, a traction-free boundary condition as described by Gresho [17,18] is used such that

$$\sigma_{ij} \cdot n_j = 0, \quad (29)$$

where σ_{ij} is the stress tensor given by

$$\sigma_{ij} = -p\delta_{ij} + \nu\left(\frac{\partial u_i}{\partial x_j} + \frac{\partial u_j}{\partial x_i}\right), \quad (30)$$

n_j is the unit vector normal to the boundary and ν is the kinetic viscosity. The main advantage of this traction-free boundary condition over a free-slip boundary condition is that velocity entrainment across the boundary is allowed.

At the outflow boundary, a non-reflective open boundary condition [19] is used where the coherent structures can be transported downstream without any distortion according to

$$\frac{\partial \Phi}{\partial t} + U_{\text{con}}\frac{\partial \Phi}{\partial x} = C_1\frac{1}{Re}\nabla^2\Phi, \quad (31)$$

where Φ is the unresolved variables, U_{con} is the area weighted mean stream-wise velocity over the outflow boundary and the coefficient C_1 is set as 0.5 in the present paper.

For T and Y_s, inlet boundary is set to satisfy the Dirichlet condition and zero gradient condition is set on the lateral boundaries. The non-reflective open boundary condition is also used at the outflow boundary.

3. Results and discussions

In order to validate our simulation, a test is first performed with the same condition as those of James and Jaberi's DNS calculation [20]. The composition of the fuel stream is 20% CH_4 and 80% N_2, and that of the oxidizer stream is 50% O_2 and 50% N_2. The velocities of the jet and co-flow streams are 100 and 50 m s^{-1} respectively. The Reynolds number based on the half jet width and inlet velocity is 3500. The reduced four-step reaction mechanism of methane–air adopted in their DNS calculation is the same as that used in our simulation. Distributions of time-averaged temperature and species mass fraction at axial location of $x = 4d$ are given in Fig. 2. The present simulation results using LES are in good agreement with the DNS results.

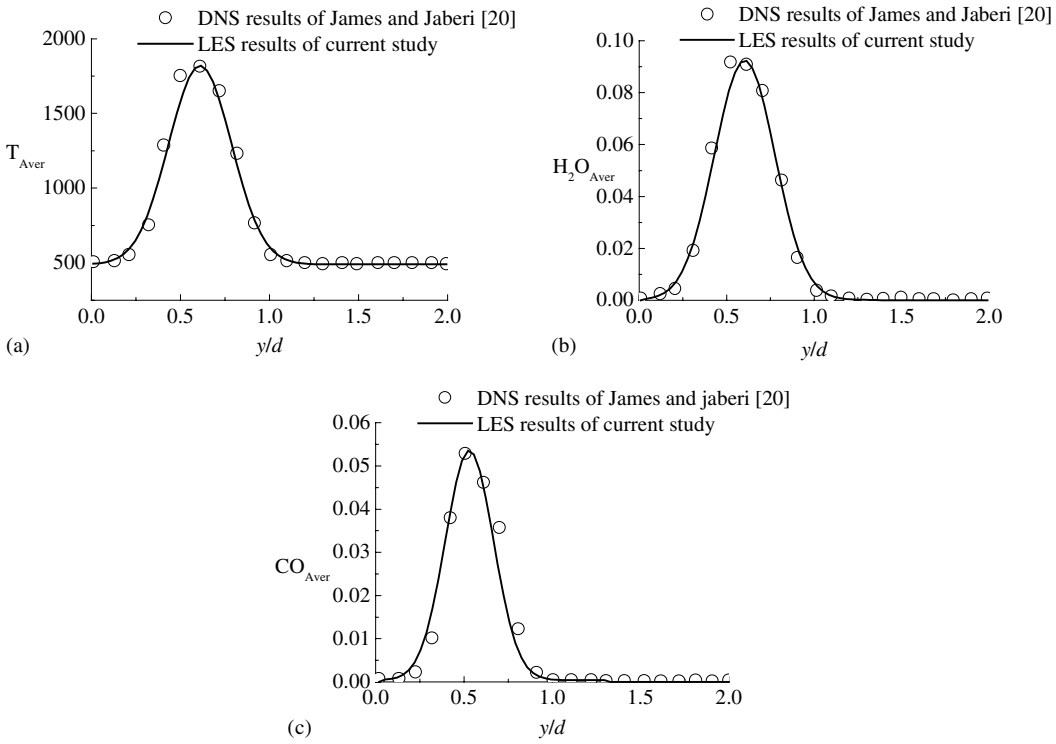

Fig. 2. Distribution of temperature and species at $x = 4d$.

Our simulation results at conditions mentioned above depict different stages of development for a diffusion jet flame and the ignition process is clearly shown in Fig. 3 where the flame is represented by its temperature contours. The coordinates shown in the figure are non-dimensional, with the horizontal coordinates representing the stream-wise direction and the vertical coordinates representing the transverse direction. The centerline of the jet is at a non-dimensional value of $y = 17$. In our numerical simulation, ignition is simulated by setting a small high temperature region of several grid sizes near the jet exit as the initial condition. Regions near the initial high temperature area are heated by the transport and diffusion of flow that carries the species along simultaneously. When the temperature and concentration of species satisfy the ignition condition, reaction begins and develops into a typical cone-shape flame front.

Figs. 4 and 5 show the transient vortical structures of the diffusion jet flame at two instances after ignition. The results illustrate the flame development in two distinct phases. The initial phase can be referred to as an underdeveloped phase as indicated in Fig. 4. Fig. 4a shows the flame structures (or state of chemical reactions) expressed as temperature contours. Fig. 4b shows the corresponding vorticity contours, which indicate the structures of the flow field. Fig. 4c and d show the distributions of mass fraction of CH_4 and CO_2. In this phase, mixing of fuel and oxidant is incomplete and combustion is at its initial stage. There exists a large amount of unburnt methane inside the flame region.

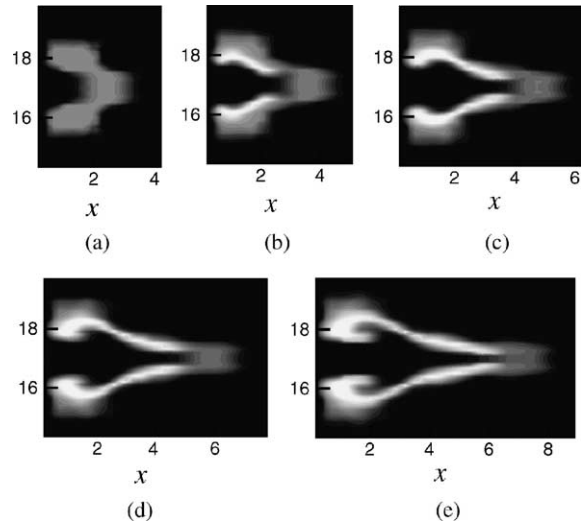

Fig. 3. Contours of temperature during ignition of the jet diffusion flame.

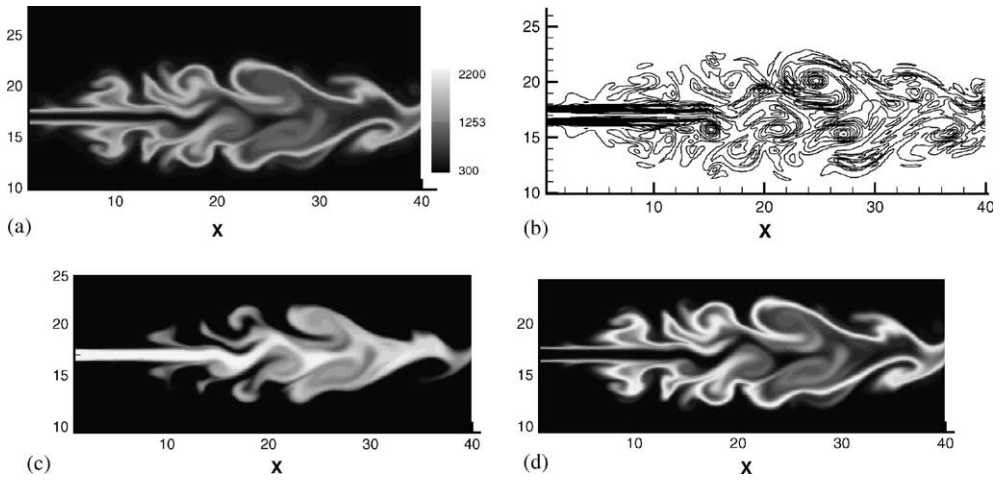

Fig. 4. Transient structures of jet diffusion flame at $t = 6.0 \times 10^{-2}$ s: (a) contours of temperature, (b) contours of vorticity, (c) contours of mass fraction of CH_4 and (d) contours of mass fraction of CO_2.

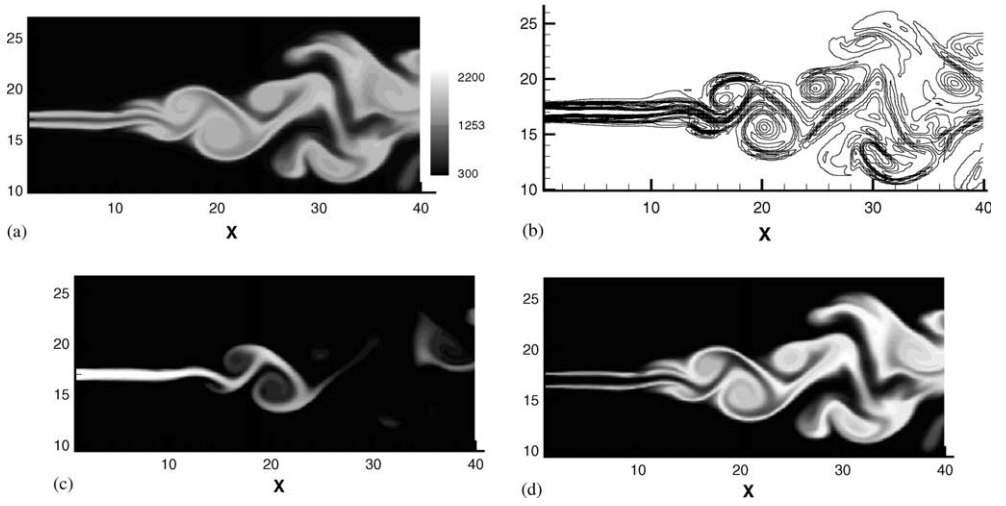

Fig. 5. Transient structures of jet diffusion flame at $t = 2.2 \times 10^{-1}$ s: (a) contours of temperature, (b) contours of vorticity, (c) contours of mass fraction of CH_4 and (d) contours of mass fraction of CO_2.

CO_2 is mainly present at the interface between the jet and its co-flow. Accordingly, the high temperature region where combustion takes place is mainly at the interface and temperature in other regions of the flow field is not high enough to sustain combustion. However, the large temperature gradient inside the flame region causes heat diffusion and some reactions exist in certain small regions of fuel and oxidant mixture. These cause the gas to expand rapidly and form instantaneously some low-density regions of small length scale. Vortices of these small scales are thus generated and these vortical structures effectively enhance turbulent mixing. The interface between fuel and oxidant is thus greatly increased leading to more reactions occurring simultaneously with turbulent mixing. This phenomenon is confirmed by the vorticity contours.

The vortical structures of the flow field are quite complex with the coexistence of both large and small scales. Due to the intensive interactions between the vortical structures and chemical reactions, the flow field is to a large extent dominated by the motion of vortical structures. Large velocity fluctuations exist in the flame region, and the transverse velocity fluctuation is extremely large as a result of intense turbulent mixing. Hence, this phase can be regarded as ''turbulence dominated''.

The numerous vortical structures resulted from the first phase greatly enhance turbulent mixing. With the

intensified turbulence and reaction, the flame evolves to become a fully developed flame, as shown in Fig. 5. The entire region of the flame attains an overall high temperature level instead of confining to the interface as in the case of the previous phase. The concentration of CH_4 in most of the flow field is low with CO_2 filling the flame region accordingly. This is the result of intensive mixing of fuel and oxidant and active chemical reactions with rapid combustion. From the distribution of vorticity, it can be seen that most vortices in the flow field have a large scale, and those small-scale vortices appearing in the previous phase are no longer present. The distribution of transient velocity distribution shows a similar behavior. Both the stream-wise and transverse velocity fluctuations are rather weak compared with those of the previous phase and combustion is much more intensive and this phase can be regarded as "reaction dominated".

In order to further illustrate the above discussion, non-dimensional turbulent kinetic energy q and reaction rate ω at different instances and locations are shown in Figs. 6–8. The three stream-wise positions selected are $x = 5d$, $x = 8d$ and $x = 11d$ respectively. The time chosen for these comparison are $t = 6 \times 10^{-2}$ s, $t = 2.2 \times 10^{-1}$ s, $t = 2.6 \times 10^{-1}$ s and $t = 3 \times 10^{-1}$ s. The first two instances are purposely chosen to be the same as those of the results given in Figs. 4 and 5, representing the "turbulence dominated" phase and "reaction dominated" phase respectively. In Figs. 6–8, turbulent kinetic energy as given by $q = (u'^2 + v'^2)/2$ is shown along the transverse position $\eta = y/(x - x_0)$, where y is the distance from the centreline of the jet, x_0 is the virtual initial point of the jet with $x_0 = -2d$. u' and v' are the non-dimensional stream-wise and transverse fluctuating velocity components respectively. It can be seen that the turbulent kinetic energy at $t = 6 \times 10^{-2}$ s at all three positions are higher than those at the other three instances. This indicates that the "turbulence dominated" phase exists only for a very short period of time, within one-tenth of a second after ignition, and the flow field is more turbulent during this phase than during the "reaction dominated" phase. For $t \geqslant 2.2 \times 10^{-1}$ s, the turbulent kinetic energy changes very little with time suggesting that the flame has remained in the "reaction dominated" phase since its full development. Therefore, the turbulent fluctuation in the initial "turbulence dominated" phase is much higher than that in the fully developed "reaction dominated" phase.

For reaction rate, Figs. 6–8 indicate that for the "turbulence dominated" phase, high values of reaction rate exist only at regions away from the centerline, indicating that reactions occur mainly at the interface of the jet and its co-flow. While for the "reaction dominated" phase, large values of reaction rate exist mainly inside the flame regions near the jet centerline. Furthermore, maximum values of the reaction rate in the "reaction dominated" phase are much higher than those of the "turbulence dominated" phase. These show that intensive reactions occur in the entire regions of the flame during the "reaction dominated" phase, which is consistent with the various plots in Fig. 5.

To further illustrate the above discussion, simulation result of a non-reactive isothermal jet at $T = 300$ K with the same initial and boundary velocity conditions of the jet flame is also given in Fig. 9. It can be seen that the vortical structures of a non-reactive jet are more complex than those of the reactive jet. Simulation result shows more small vortices in the non-reactive jet and the gradient of the vorticity is obvious larger than that of the reactive jet. Fig. 9 shows that the jet flame is less turbulent than the isothermal jet at the same velocity condition, consistent to the above discussions.

Result of simulation without SGS reaction model is also given in Fig. 10. It shows that the non-SGS calculation gives unsatisfactory result. The shape of the flame is to some extent unreasonable as less vortical structures and flame details are captured compared to the results obtained using the SGS model.

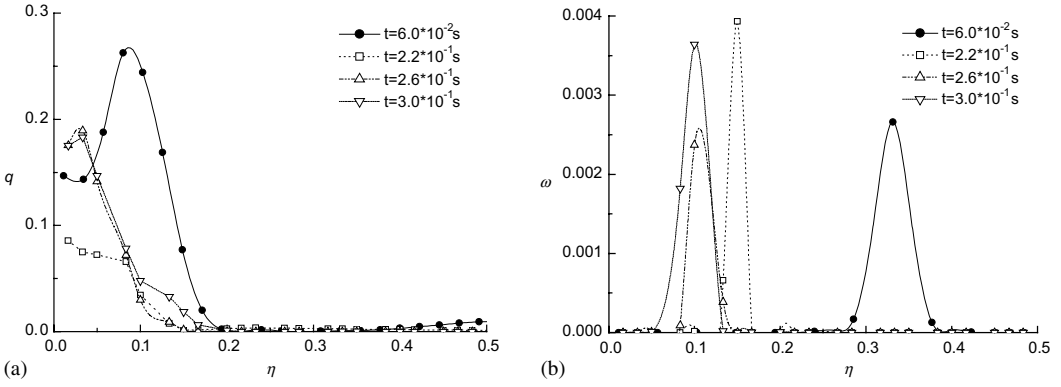

Fig. 6. Turbulent kinetic energy and reaction rate at $x = 5d$.

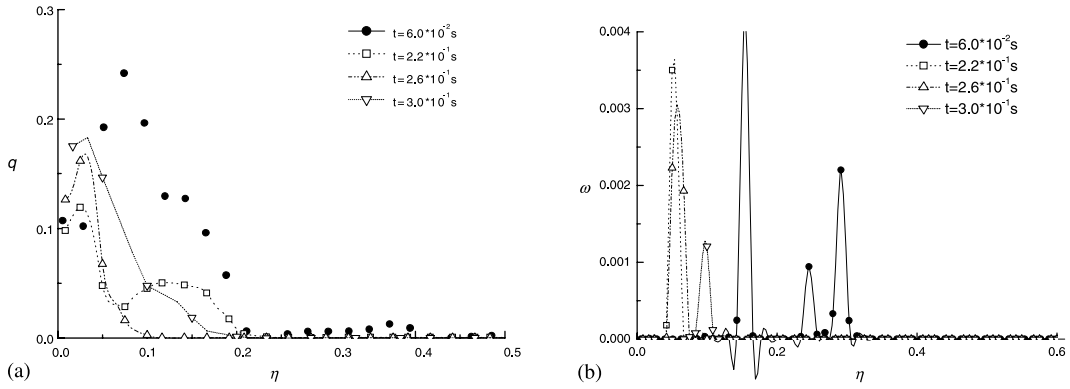

Fig. 7. Turbulent kinetic energy and reaction rate at $x = 8d$.

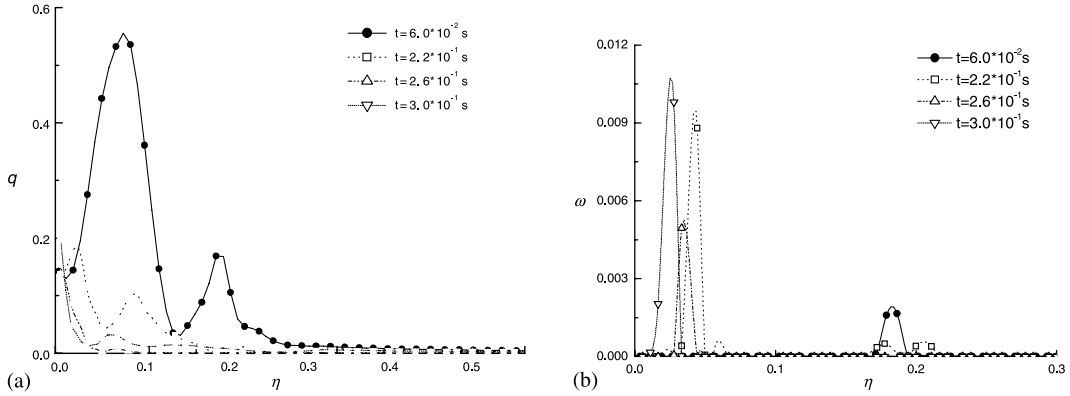

Fig. 8. Turbulent kinetic energy and reaction rate at $x = 11d$: (a) turbulent kinetic energy and (b) reaction rate.

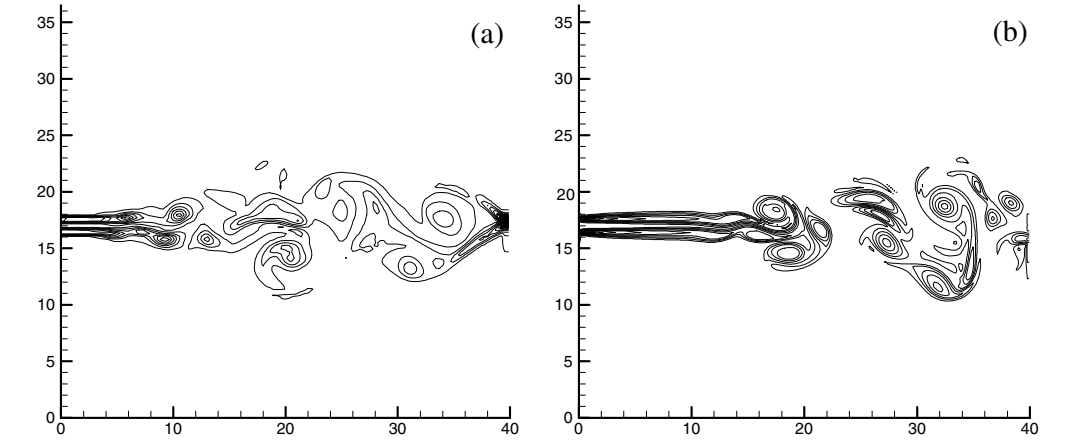

Fig. 9. Comparison between reactive and non-reactive jet at $t = 1.0 \times 10^{-1}$ s: (a) contours of reactive jet and (b) contours of non-reactive jet.

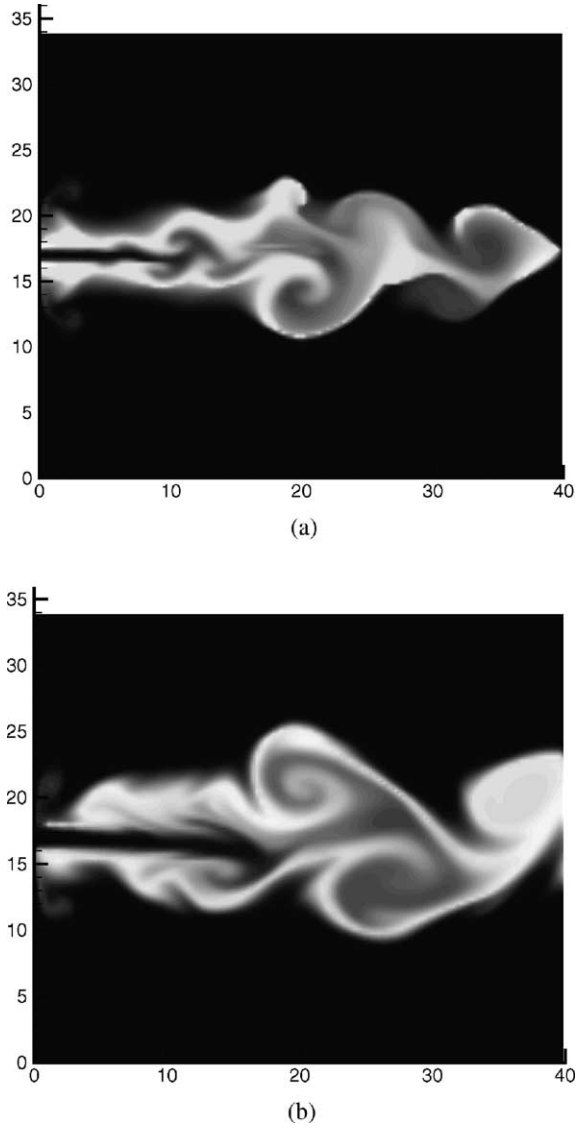

Fig. 10. Comparison between simulation results of with and without SGS mode at $t = 1.0 \times 10^{-1}$ s: (a) contours of temperature with SGS reaction model and (b) contours of temperature without SGS reaction model.

4. Conclusions

In this paper, an efficient LES code is used to simulate a two-dimensional spatially developing transitional jet diffusion flame of methane at moderate Reynolds number. Simulation results show different features of the diffusion flames, with the ignition process well illustrated. Detailed description of transient vortical structures in the entire flow field is given together with the transient interactions between vortical structures and chemical reactions. The development of a diffusion jet flame is found to involve two distinct phases. The first is a very short initial developing phase when intensive vortex–flame interactions occur with the formation of many small-scale vortical structures in the flow field and comparatively high turbulent kinetic energy. This phase is regarded by the authors as "turbulence dominated". The other phase is a fully developed combustion phase where vortical structures of the flame are rather less "turbulent" with rapid combustion and is regarded by the authors as "reaction dominated".

Acknowledgements

This work was partially supported by the Research Committee of The Hong Kong Polytechnic University (Project G-YC18), the National Natural Science Foundation of China (Grant no. 50006006), and the Tsinghua University Graduate School Ph.D. Thesis Foundation.

References

[1] C.F. Kaminski, X.S. Bai, J. Hult, Flame growth and wrinkling in a turbulent flow, Appl. Phys. B 71 (2000) 711–716.
[2] C.J. Mueller, R.W. Schefer, Coupling of diffusion flame structure to an unsteady vortical flow field, in: Twenty-Seventh Symposium (International) on Combustion, The Combustion Institute, Pittsburgh, 1998, pp. 1105–1112.
[3] V.R. Katta, K.Y. Hsu, W.M. Roquemore, Local extinction in an unsteady methane–air jet diffusion flame, in: Twenty-Seventh Symposium (International) on Combustion, The Combustion Institute, Pittsburgh, 1998, pp. 1121–1129.
[4] J.E. Rehm, N.T. Clemens, The large-scale turbulent structure of nonpremixed planar jet flames, Combust. Flame 116 (1999) 615–626.
[5] G.L. Brown, A. Roshko, On density effects and large structure in turbulent mixing layers, J. Fluid Mech. 64 (4) (1974) 775–816.
[6] C.D. Winant, F.K. Browand, Vortex pairing: the mechanism of turbulent mixing-layer growth at moderate Reynolds number, J. Fluid Mech. 63 (2) (1974) 237–255.
[7] A. Lingeus, Instability of buoyant diffusion flame, Exp. Fluids 20 (1996) 241–248.
[8] J.E. Rehm, N.Y. Clemens, The relationship between vorticity/strain and reaction zone structure in turbulent non-premixed jet flames, in: Twenty-Seventh Symposium (International) on Combustion, The Combustion Institute, Pittsburgh, 1998, pp. 1113–1120.
[9] J. Warnatz, in: W.C. Gardiner (Ed.), Combustion Chemistry, Springer-Verlag, Berlin, 1984, pp. 197–360.
[10] C. Fureby, On subgrid scale modeling in large eddy simulations of compressible fluid flow, Phys. Fluids 8 (5) (1996) 1301–1311.
[11] F.A. Jaberi, S. James, A dynamic similarity model for large eddy simulation of turbulent combustion, Phys. Fluids 10 (7) (1998) 1775–1777.

[12] K. Seshadri, N. Peters, Asymptotic structure and extinction of methane–air diffusion flames, Combust. Flame 73 (1988) 23–44.
[13] M. Germano, U. Piomelli, P. Moin, H.C. William, A dynamic subgrid-scale eddy viscosity model, Phys. Fluids A—Fluid Dynamic 3 (7) (1991) 1760–1765.
[14] J. Smagorinsky, General circulation experiments with primitive equations, Monthly Weather Rev. 91 (3) (1963) 99–164.
[15] G. Erlebacher, M.Y. Hussaini, C.G. Speziale, T.A. Zang, Towards the large-eddy simulation of compressible turbulent flows, J. Fluid Mech. 238 (1992) 155–185.
[16] F.O. Thomas, Structure of mixing layers and jets, Appl. Mech. Rev. 44 (3) (1991) 119–153.
[17] P.M. Gresho, Some current CFD issues relevant to the incompressible Navier–Stokes equations, Comp. Meth. Appl. Mech. Eng. 87 (1991) 201–223.
[18] P.M. Gresho, Incompressible fluid dynamics: some fundamental formulations issues, Ann. Rev. Fluid Mech. 23 (1991) 413–426.
[19] Y. Dai, T. Kobayashi, N. Taniguchi, Large eddy simulation of plane turbulent jet flow using a new outflow velocity boundary condition, JSME Int. J. Ser. B—Fluids Thermal Eng. 37 (2) (1994) 242–253.
[20] S. James, F.A. Jaberi, Large scale simulations of two-dimensional nonpremixed methane jet flames, Combust. Flame 23 (2000) 465–487.